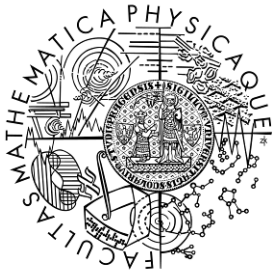

FACULTY
OF MATHEMATICS
AND PHYSICS
Charles University

BACHELOR THESIS

Marius Hegedüs

Mechanical properties of pre-compressed Mg-Zn-Ca alloy

Department of Physics of Materials

Supervisor of the bachelor thesis: doc. Ing. Patrik Dobroň, Ph.D.

Study programme: Physics

Specialization: Applied Physics

Prague 2018

I declare that I carried out this bachelor thesis independently, and only with the cited sources, literature and other professional sources.

I understand that my work relates to the rights and obligations under the Act No. 121/2000 Coll., the Copyright Act, as amended, in particular the fact that the Charles University has the right to conclude a license agreement on the use of this work as a school work pursuant to Section 60 paragraph 1 of the Copyright Act.

In Prague, 17.5.2018 Marius Hegedüs

First of all, I would like to thank my thesis supervisor doc. Patrik Dobroň, for his guidance, time and attention he has given me and my bachelor thesis. My thanks also belong to my thesis advisor Daria Drozdenko who was always helpful towards me throughout my entire research. Furthermore, I would also like to thank Peter Harcuba and Klaudia Horváth for providing me with useful information about acquisition and processing of scanning electron microscopy data Jana Kálalová and Marta Čepová for providing me with knowledge and training necessary for sample preparation. As well as to all other members of the department who never hesitated to offer me their help and expertise.

This bachelor thesis was completed within the framework of the research grant No. 17-21855S by the Czech Science Foundation.

Title: Mechanical properties of pre-compressed Mg-Zn-Ca alloy

Author: Marius Hegedüs

Department / Institute: Department of Physics of Materials

Supervisor of the bachelor thesis: doc. Ing. Patrik Dobroň, Ph.D.

Abstract: In wrought Mg alloys, their hexagonal closed packed structure together with a pronounced basal texture lead to anisotropy of mechanical properties. This bachelor thesis is focused on understanding the influence of previous deformation with further relaxation and/or additional heat treatment on deformation behaviour of the extruded Mg-Zn-Ca alloy. The significant influence of twins formed after pre-compression on mechanical properties was investigated. Evolution of microstructure, especially a formation of twins, is observed by light and scanning electron microscopy. The acoustic emission technique is used to determine active deformation mechanisms: dislocation slip and twinning. The results can be used for developing Mg alloys with enhanced properties.

Keywords: magnesium alloys, twinning, precipitation, mechanical properties

Contents

Introduction **1**

1. Theoretical part **2**

1.2. Plastic deformation of metals with hexagonal crystal structure 2

1.3. Strengthening via thermomechanical treatment 6

1.3.1 Influence of deformation twinning on strain hardening 6

1.3.2 Precipitation Hardening 6

1.4. Extrusion 8

1.5. Acoustic emission 9

2. Aims and objectives **10**

3. Experimental procedure **11**

3.1. Material 11

3.2. Deformation tests 11

3.3. Acoustic emission 12

3.4. Microscopy 13

3.4.1. Light microscopy 13

3.4.2. Scanning electron microscopy 13

4. Results **15**

5. Discussion **25**

Conclusions **29**

Bibliography **30**

List of Tables **33**

List of Abbreviations **34**

Introduction

Magnesium is a chemical element with atomic number 12. It is a metal with shiny grey colour. Magnesium is ninth most abundant element in the universe [1] as well as the eighth most abundant element in the Earth's crust (2.1%) [2]. It naturally occurs only in combination with other elements with +2 oxidation states. Its density at room temperature (RT) is $1.738\ g.cm^{-3}$ with melting point at 650°C [3] Thanks to its crystallisation in hexagonal close packed (HCP) structure (Fig. 1.3) it exhibits a highly anisotropic behaviour. Magnesium is easily obtainable from seawater as 1,3 kg of magnesium can be extracted from 1 m^3 of seawater [2].

Magnesium alloys are, thanks to their lower density than commonly used steels or aluminium alloys, the lightest structural metals. This makes them suitable for variety of industrial applications including electronics where magnesium alloys are utilized as a replacement for plastics due to its weight. Moreover, in comparison with polymers, magnesium alloys have better mechanical properties, better resistance to aging and better thermal conductivity, making them ideal for use in portable electronics. In automotive and aerospace sector, construction of parts from magnesium alloys leads to significant weight reduction positively influencing overall fuel efficiency. High damping capability of magnesium alloys is making them a great absorbent of energy, what can be utilized in deformation zones of vehicles. Recycling of magnesium alloys is also very energy efficient, as recycling magnesium alloys only requires 5% of the energy required to produce primary magnesium alloys. Moreover, magnesium and its alloys are biocompatible and biodegradable materials, thus promising for medical applications. The density of magnesium ($1.738\ g.cm^{-3}$ [3]) is the closest to human bone density ($1.9\ g.cm^{-3}$ [4]) in comparison to all metals used as implants. Recently, in vivo investigations of a rat femur implantation [5] showed very promising results for the ZX10 alloy.

Therefore, it is important to understand deformation behaviour of magnesium alloys and ways to improve their properties. Obtained knowledge can help to develop novel magnesium alloys with enhanced properties for broad spectrum of industrial applications.

1. Theoretical part

1.2. Plastic deformation of metals with hexagonal crystal structure

Deformation behaviour of crystalline materials is significantly influenced by crystallographic defects. Dislocation is a line defect in regular crystal structure, around which some atoms of lattice are misaligned. There are two basic types of dislocations, *edge* (Fig. 1.1 a) and *screw* (Fig. 1.1 b).

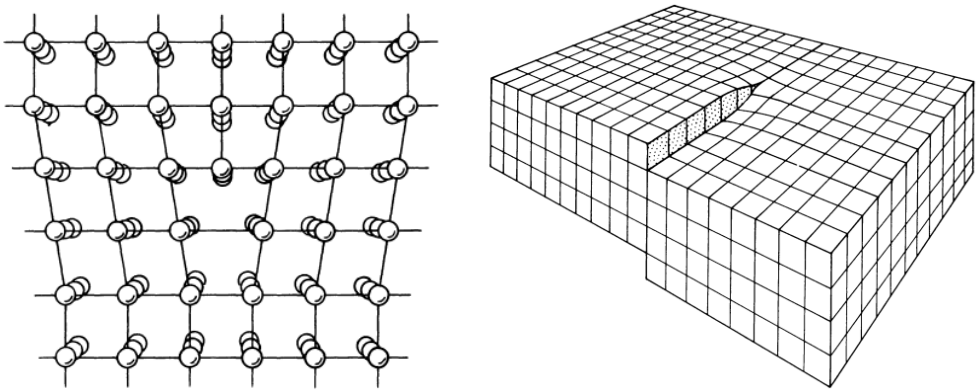

a) b)

Fig. 1.1: Edge dislocation [6]

We can imagine edge dislocation as an end of extra plane of atoms being introduced midway through the crystal, which causes distortion of nearby atomic planes. Screw dislocation is more difficult to visualize. We can imagine cutting the crystal and slipping one half across the other along the dislocation line. With applying external force, dislocations can be created and set in motion (Fig. 1.1 b) [6].

Basically, plastic deformation in HCP metals is performed by collective motion of dislocations (dislocation slip) and twinning. The dislocation slip (Fig. 1.2) occurs in directions and planes with the densest occupation of atoms where shear stress τ is the greatest. According to Schmid's law, this value is independent of external stress and depends on orientation of slip system towards applied force [7].

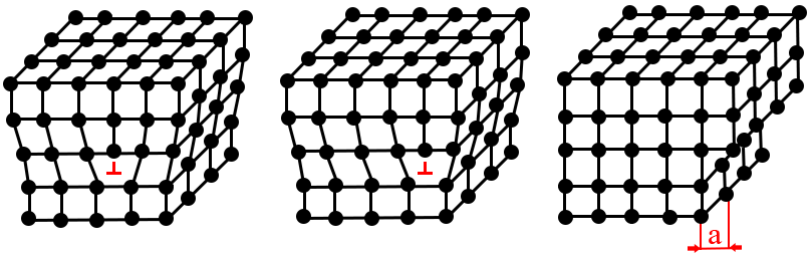

Fig. 1.2 Movement of edge dislocation

In materials with HCP lattice (Fig. 1.3), the activation of particular slip system depends on the *c/a* ratio. The ideal *c/a* ratio is $\sqrt{\frac{8}{3}} \approx 1.6329$. Magnesium has the *c/a* ratio of 1.6236 [8]. Therefore, primary slip is basal slip and it is performed on the (0001) basal plane in the <11-20> direction. Secondary slip (prismatic slip) occurs in the <11-20> direction on the {10-10} planes. At elevated temperatures, slip can also be performed in the <11-20> direction on the {10-11} pyramidal planes [9] (Fig. 1.4). Therefore, magnesium alloys have low plasticity at RT.

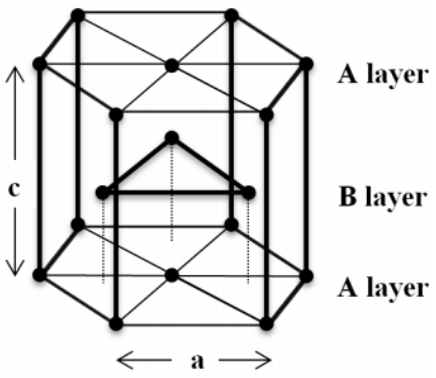

Fig. 1.3 Hexagonal close packed lattice structure [8]

The amount of possible slip systems influences the ability of material to deform, which impacts its overall mechanical properties. According to von Mises criterion for homogeneous plastic deformation in polycrystals, the existence of five independent slip systems is required [10]. To fulfil Von Mises's criterion in Mg and its alloys another deformation mechanism needs to be activated. This mechanism is called twinning.

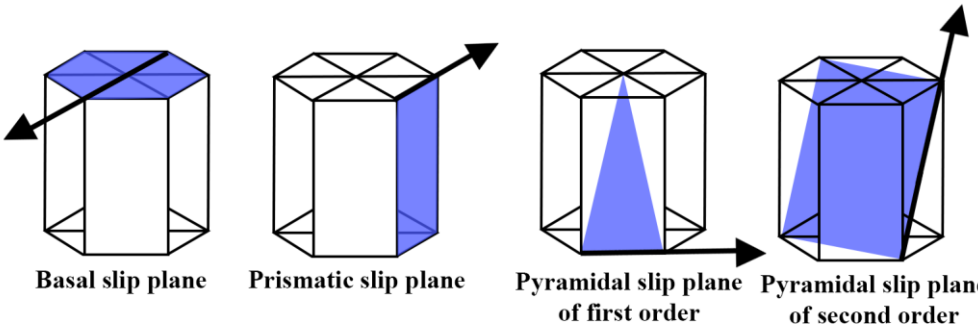

Fig. 1.4: Basic slip planes in hexagonal metals

A shear force can produce atomic displacements what leads to formation domain inside original grain, which share the same crystal lattice in a symmetrical manner and are separated by twin plane – twin boundary. Mechanical twinning is schematically illustrated in Fig. 1.5, where open circles represent atoms that did not change position, and solid circles represent final position of atoms after shearing. [11]

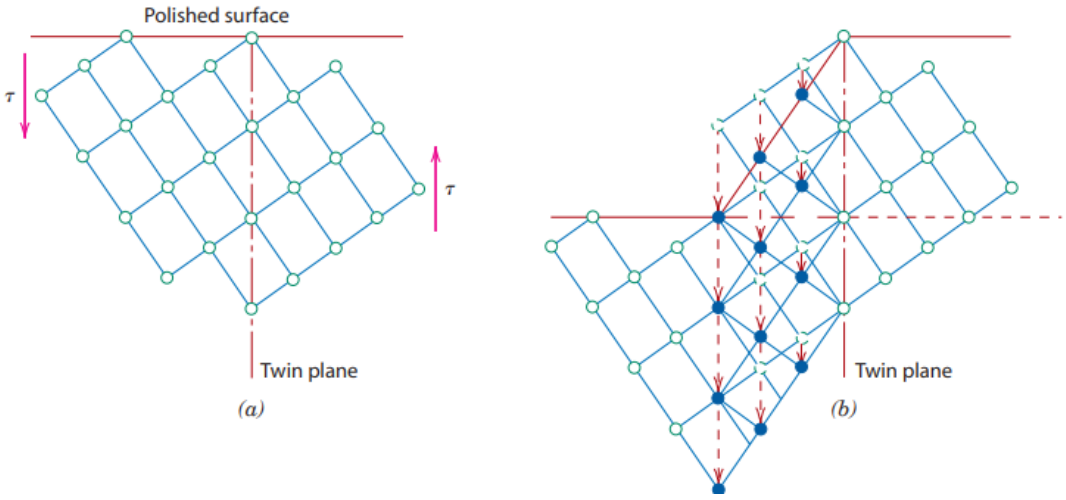

Fig. 1.5 Schematic diagram of twinning process [11]

In magnesium, most common type of twinning system is the {10-12} <10-11> extension twinning and it is characterised by angle of misorientation with respect to original crystallographic plane of 86.3° [12]. Those twins are formed when the *c*-axis is oriented perpendicular to axis of applied compressive stress [13], Fig. 1.6.

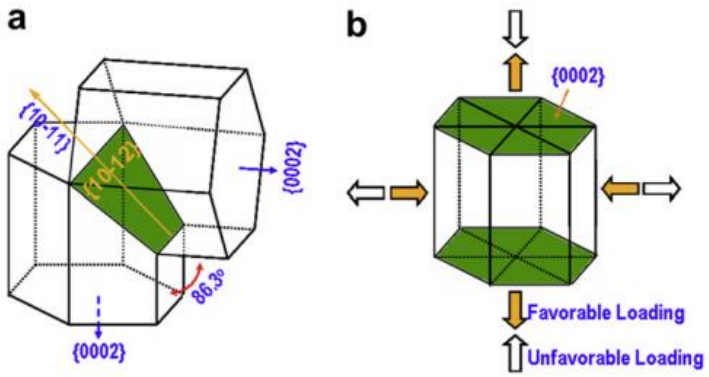

Fig. 1.6 Illustration of {10-12} <10-11> extension twin formation [14]

Polycrystalline materials are composed of many crystallites of various size and orientation - grains. The grain size of polycrystalline material influences its mechanical properties. Adjacent grains usually have different crystallographic orientations and a common grain boundary [11], as illustrated in Fig. 1.7.

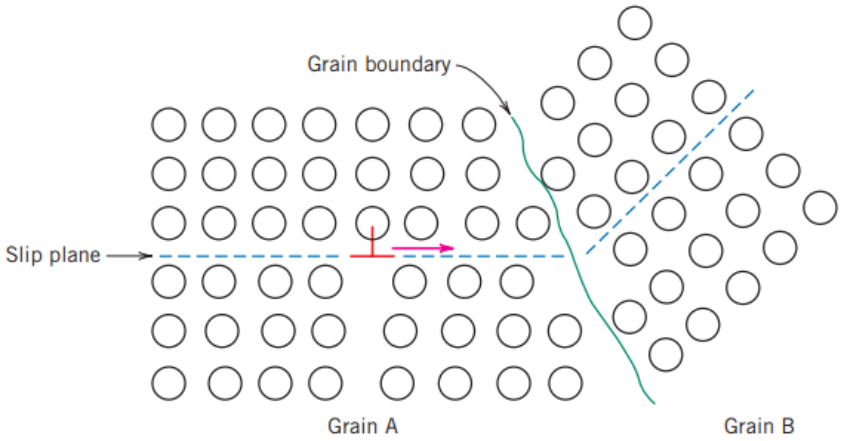

Fig. 1.7 Movement of a dislocation across the grain boundary. [15]

During plastic deformation, dislocation motion must take place across this common boundary, as indicated in Fig. 1.7, from grain A to grain B. The boundary acts as a barrier to dislocation motion. Since the two grains possess different crystallographic orientations, a dislocation passing into gran B will have to change its direction of motion. This process becomes more energetically demanding with increase of crystallographic misorientation inside the grains. Also, the atomic disorder within a grain boundary region results in discontinuity of slip planes from one grain into the other one.

In the case of high-angle grain boundaries, dislocations tend to pile up at grain boundaries rather than transverse them. These pile-ups induce stress concentration ahead of their slip planes, which generate new dislocations in adjacent grains.

The fine-grained material has greater total grain boundary area to impede dislocation motion. Dependence of grain size on strength of material can be described by Hall-Petch law:

$$\sigma_y = \sigma_0 + k_y d^{-\frac{1}{2}} \quad (1)$$

where σ_y is yield strength, d is average grain diameter, and σ_0 and k_y are constants for a particular material [11].

1.3. Strengthening via thermomechanical treatment

1.3.1 Influence of deformation twinning on strain hardening

Besides the grain boundaries, mechanical twins by introducing twin boundaries, present another obstacle in the way of moving dislocations. Therefore, the introducing of twins into material can lead to further increase its hardness. According to [16] these physical mechanisms appear to be associated with deformation twinning:

a) *Strengthening effect* caused by reduction of the free path of moving dislocation (distance that dislocation can travel without encountering an obstacle, e.g. in from of grain or twin boundary). This is also referred to as *Hall-Petch effect* that is described by (1). *Basinski mechanism* contributes by transformation of glissile dislocations to sessile dislocations inside the twins.

b) *Textural softening* caused by reorientation of the grain lattice to a more favourable orientation for dislocation slip.

1.3.2 Precipitation Hardening

If the neighbouring grains do not differentiate only in orientation but also in crystallographic structure or composition, these two grains represent two different phases (for example, α and β). Small volumes of β phase are normally formed in the space between three grains of α phase, as seen in Fig. 1.8, due to minimal energy [7].

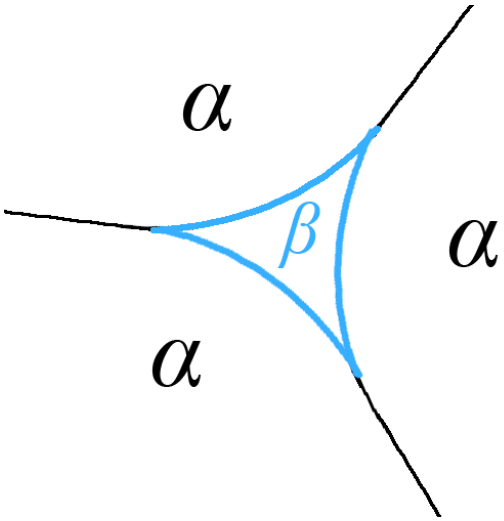

Fig. 1.8 Point of contact of three grains in material with two phases

It is possible to enhance hardness of magnesium alloys by formation of small uniformly dispersed particles (precipitates) of a second phase within the original phase matrix. This is accomplished by phase transformations induced by appropriate heat treatment [11]. Those precipitates, similar to grain and twin boundaries, form obstacles on the way of moving dislocations. Example of edge dislocation interacting with precipitate is displayed in Fig. 1.9.

Structural relationship between crystallographic structures of two phases determine the type of interface between the phases and affect the final shape of particle [7].

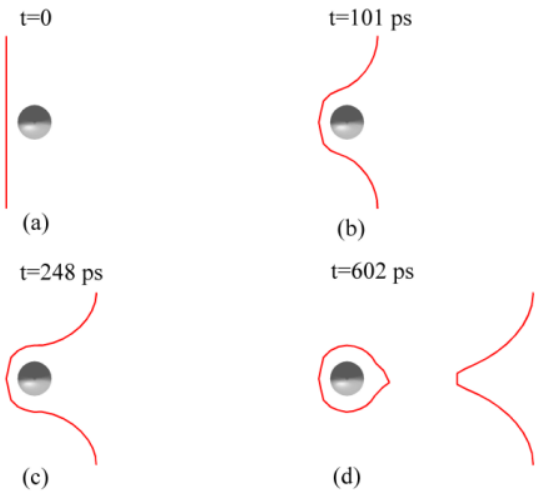

Fig. 1.9: Edge dislocation interacting with a precipitate. [17]

1.4. Extrusion

Extrusion is a method of thermomechanical processing which is widely used for magnesium and its alloys. This process creates profiles with fixed cross-section. Material is pushed through a die of a desired form of cross-section by a ram. Extrusion process is schematically displayed in Fig. 1.10. Extrusion parameters have significant impact on microstructure of material. It is mainly used to refine the grain size, what results in hardening of material. The important parameters of extrusion are the extrusion temperature, the extrusion rate and the extrusion ratio. Based on extrusion temperature, the extrusion can be cold, warm or hot. Cold extrusion is performed at temperature close to RT. Warm extrusion is done in range from RT up to recrystallization temperature. Hot extrusion is performed at temperatures above the recrystallization temperature [8].

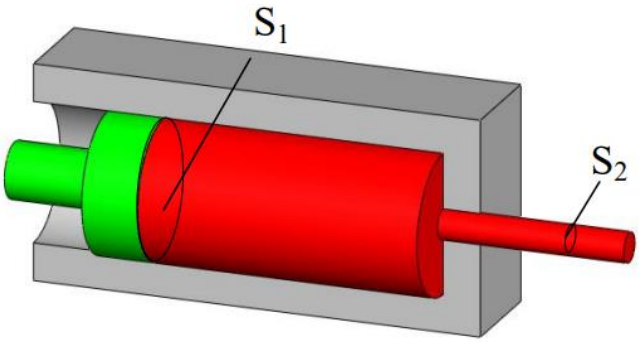

Fig. 1.10 Schematic interpretation of extrusion process. [8]

The optimal extrusion rate is experimentally determined value. Each alloy has its optimal extrusion rate which achieves best mechanical properties after extrusion. The extrusion rate significantly depends on the extrusion temperature. In general, higher the temperatures allow for higher extrusion rates [8].

The extrusion ratio (ER) can be defined as:

$$ER = \frac{S_2}{S_1} \tag{2}$$

where S_1 is the initial cross-section and S_2 is the final cross-section.

Magnesium alloys are usually extruded above recrystallisation temperature (hot extrusion) in range between 300-400°C [8].

Extruded Mg alloys are usually characterised by texture with a distinct alignment of basal planes parallel to the extrusion direction (ED) [18]. Considering that twinning is orientation dependent process (for activation of the {10-12} <10-11>

extension twinning compression needs to be applied perpendicular to c-axis) extension twins are preferentially activated during compression along ED.

1.5. Acoustic emission

Acoustic emission (AE) is the phenomenon of propagation of transient elastic waves within the material due to a local dynamic change with a sudden release of energy. These elastic waves have its characteristic parameters, based on which we can determine the type of the deformation mechanism, dislocation slip or the formation of mechanical twins.

The advantages of this technique are that it is passive, non-destructive method and measurements can be performed during deformation tests, so called *in-situ*, i.e. data can be processed and evaluated in real time. Therefore, it is suitable to determine active deformation mechanisms during deformation tests.

We recognize two types of the AE signal according to their characteristics, continuous and discontinuous. If the elastic wave is generated from a large number of sources, has low energy and the amplitude of AE does not drop below certain level it is called continuous AE. When the signals are separated in time with large energy, it is a discontinuous AE. Sources of continuous emission in metals are correlated with micro-mechanisms influencing the plastic deformation. The most significant role in plastic deformation have dislocations and its stress fields that are able to generate AE. It is important to note that AE is only able to capture collective dislocation motion [19, 20]. Other sources of AE include processes during which internal stresses in material are released e.g. during recrystallization. Discontinuous AE is generated as a result of unstable character of plastic deformation or as a result of degradation processes in material such as corrosion or formation of cracks. Unstable character of plastic deformation is in some materials manifested by twinning or movement of large sums of dislocations. However, AE can only capture the nucleation of twins, not their growth [20].

Disadvantage of AE technique is background noise and therefore, low sensitivity to processes during which low energy levels are released [2].

2. Aims and objectives

- Determine a dependence of isothermal aging time on compressive yield strength of the pre-compressed ZX10 alloy and optimize heat treatment conditions.
- Investigate an influence of different levels of pre-compression on mechanical properties in tension and compression of the ZX10 alloy in as-extruded state and after selected heat treatment.
- Explain deformation behaviour of the ZX10 alloy with respect to microstructural changes due to thermomechanical treatment.

3. Experimental procedure

3.1. Material

The Mg-Zn-Ca (Mg + 0.9 wt.% Zn + 0.25 wt.% Ca) alloy, hereafter called ZX10, was prepared by a modified gravity casting process with directional solidification by lowering the crucible into a water bath. After machining, the billets were solid-solution annealed for 20 h at 400°C. Indirect extrusion to a round bar (extrusion ratio 1:25) with a final diameter of 10 mm was carried out at 400°C with an extrusion speed of 0.5 mm/s (ram speed, corresponding profile exit speed of 0.75 m/min). Initial texture of the extruded alloy was measured by the X-ray PANalytical XPert diffractometer using CuKα radiation on polished samples in reflection geometry to a sample tilt of 70°.

The ZX10 alloy was produced in Magnesium Innovation Centre (MagIC), Helmholtz-Zentrum Geesthacht, Germany. The texture measurement was performed at the same institute and results were provided together with the alloy.

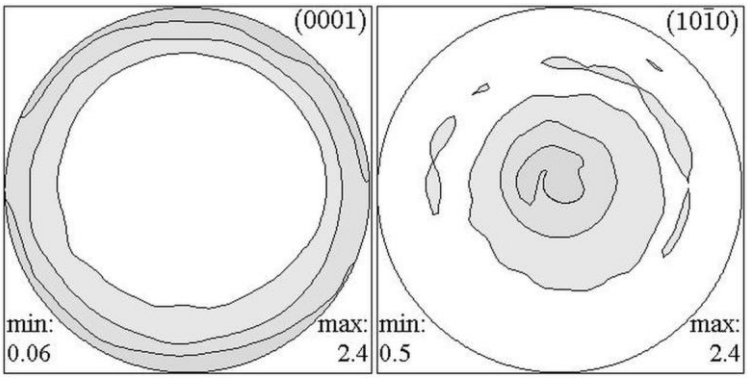

Fig. 2.1: Pole figures of the extruded ZX10 alloy (× ED)

3.2. Deformation tests

Samples were subjected to both compressive and tensile deformation tests using an INSTRON® 5882 universal testing machine (schematically illustrated in Fig. 2.2). Samples for deformation tests were machined from the round bar parallel to ED. Samples with a diameter of 9.5 mm and a gauge length of 14 mm were used for compressive deformation tests. Samples for tensile deformation tests had a diameter of 5 mm and a gauge length of 13 mm. All deformation tests were carried out at RT

and at a constant crosshead speed of $10^{-3}\ s^{-1}$. The data was recorded using the Blue Hill® software supplied by INSTRON®.

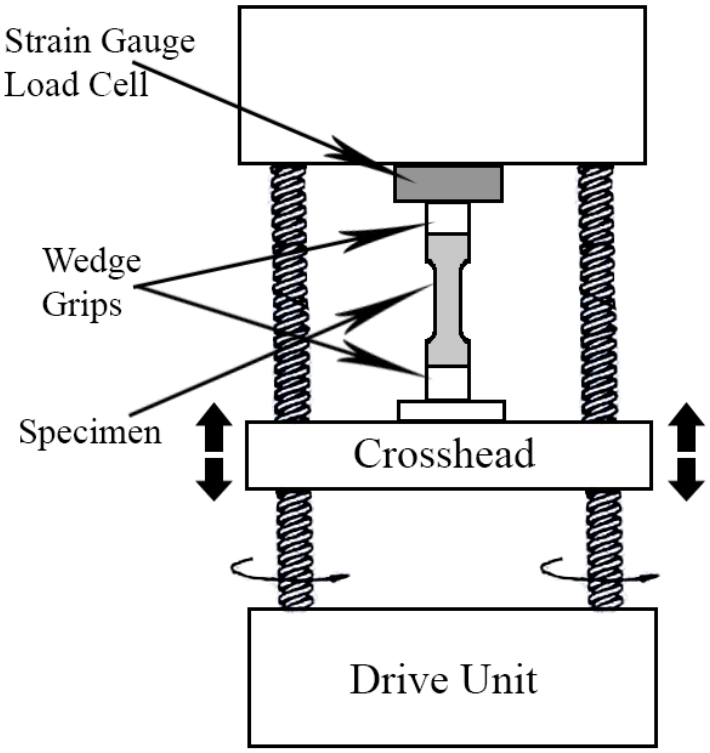

Fig. 2.2: Schematic illustration of universal testing machine INSTRON® 5882

All data obtained from deformation tests were processed in OriginPro 2015 software, true stress and strain were calculated with respect to the machine stiffness in compression or tension.

3.3. Acoustic emission

AE during deformation tests was recorded by a computer-controlled PCI-2 device from Physical Acoustic Corporation (PAC) with the sampling frequency of 2MHz. A piezoelectric transducer Pico 7553 (PAC) with a diameter of 3 mm and a relative flat frequency response in a frequency range of 100-600 kHz was attached to the sample surface using a wooden clamp. For better contact between the sample and transducer, a silicone grease was applied. The AE signal was amplified using a 2/4/6-preamplifier giving a gain of 60dB. After the measurement, threshold-level detection of recorded AE signals was done to achieve a comprehensive set of AE parameters.

The threshold voltage for the AE count rate ΔNC/Δt (number of counts per second [21]) was set to 0.1 V. The full scale of the A/D converter was 10 V.

3.4. Microscopy

Samples for both Light and Scanning electron microscopy (SEM) were ground using TegraPol 15 (Struers®) polishing machine using SiC papers with roughness up to 4000. They were subsequently polished by diamond pastes down to 0.25 μm particle size. For final polishing step OP-S suspension and Opchem polishing pad were utilized.

3.4.1. Light microscopy

Polished surfaces of samples for light microscopy were etched 5-10 seconds with picric acid etchant.

For microstructure observation, an OLUMPUS® GX51 microscope equipped with a PIXELINE® CCD camera was used. The captured images were evaluated using Nis-Elements AR software. The average grain size *d* was determined by the average grain intercept method.

3.4.2. Scanning electron microscopy

Microstructure of samples before and after pre-deformation was observed by FEI Quanta 200F scanning electron microscope (SEM). Polished samples were glued using conductive adhesive onto a metal plate, before inserting into microscope chamber. For better surface quality last step of surface preparation was Ar ion milling using Leica EM RES102. Samples were observed under acceleration voltage of 10kV.

Further analysis of microstructure and its development with respect to pre-deformation was observed using electron backscatter diffraction (EBSD) method. EBSD data were processed using OIM Analysis™ software.

As was mentioned before, the {10-12} extension twins rotate basal planes by 86.3° with respect to their original orientation. Therefore, after pre-compression along ED, newly created twins will be characterized by basal planes oriented perpendicular to ED. It makes possible to estimate twin volume fraction (TVF), which was established as fraction of the grains with their <0001> axis parallel to ED with angle tilt (to transversal direction) tolerance of 30% (Fig. 2.3).

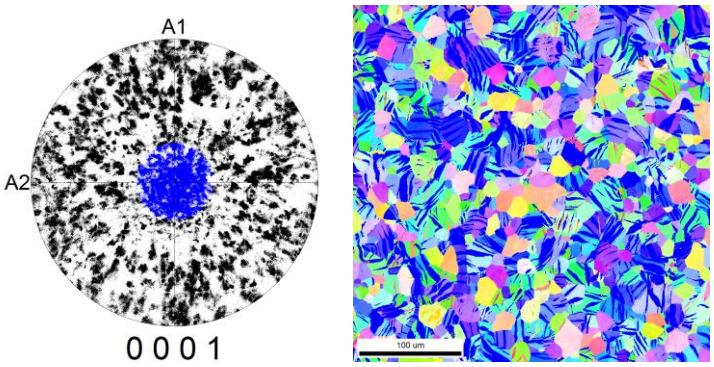

Fig. 2.3: Example of the TVF selection.

EBSD data were also subjected to kernel average misorientation (KAM) analysis. KAM quantifies the average misorientation around a measurement point with respect to a defined set of nearest neighbour points (in our case with respect to 1st neighbour). In this mode, the local misorientation assigned to the centre point of a particular grain with respect to all points in the perimeter of the kernel are measured [22].

4. Results

Microstructure of cross section of the extruded ZX10 alloy acquired by a light microscopy is displayed in Fig. 3.1. The ZX10 alloy has homogeneous microstructure with an average grain size of (15 ± 4) μm. The Mg alloy exhibits a basal texture with a distinct alignment of basal planes parallel to ED, as we can see in Fig. 2.1.

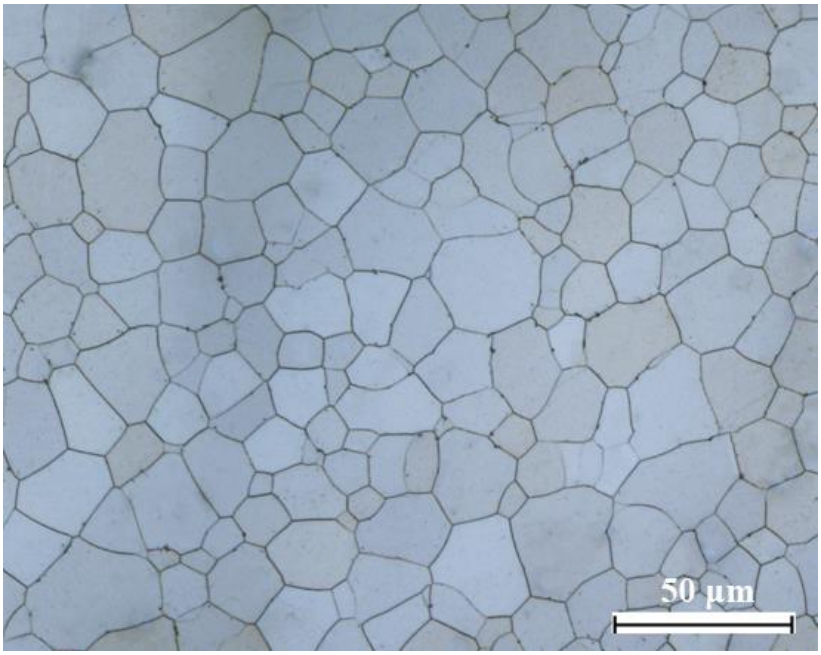

Fig. 3.1: Microstructure of the extruded ZX10 alloy provided by a light microscopy ($\times$ ED)

All deformation curves have a typical shape for polycrystalline materials with a linear region at beginning of the test corresponding to elastic deformation and macroscopic plastic deformation occurs after reaching the yield point.

As we can see in Fig. 3.2, an apparent tension–compression asymmetry in the flow stress is observed. In compression, an S-shaped deformation curve can be seen. After 4% of plastic strain, a significant strain hardening takes place. The tensile deformation curve has a convex shape. Initial yield strength in compression and in tension was calculated to be (112 ± 2) and (127±3) MPa, respectively.

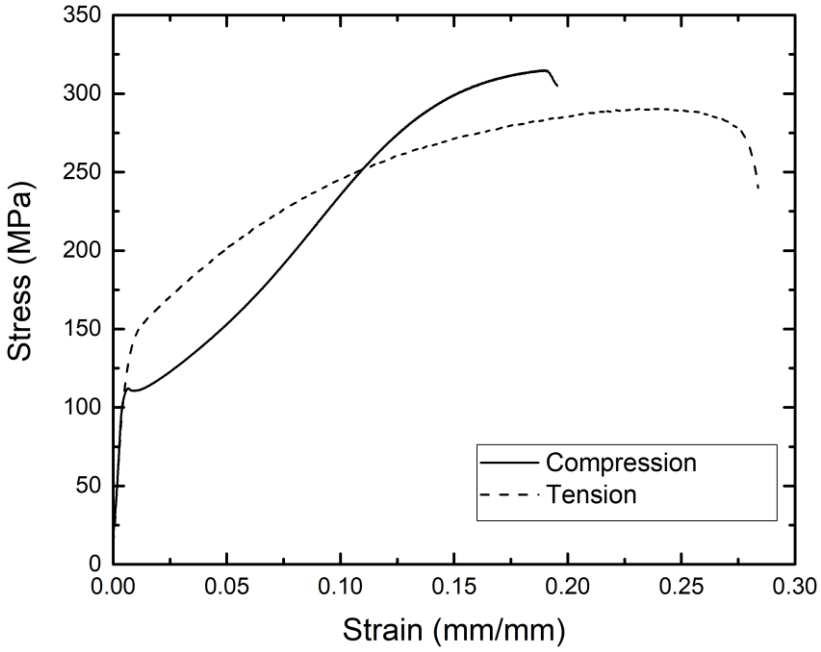

Fig. 3.2: Compressive and tensile deformation curves

AE activity in form of count rate is correlated to deformation curves of sample in as-extruded state, Fig. 3.3 and 3.4 In region of elastic deformation, we observe AE activity with its peak around macroscopic YP. With increasing plastic deformation, the AE activity is decreasing. This is common in both compression (Fig. 3.3) and tension (Fig. 3.4). Peak level of the AE count rate was observed in compression (Fig. 3.3) greater than 10^5 s^{-1}, entire magnitude higher than in tension (Fig. 3.4) with its peak at about 10^4 s^{-1}. Furthermore, we observe different character of AE in compression and tension. In compression (Fig. 3.3), the AE count rate is characterised by distinct peaks and drops in region of plastic deformation. In tension (Fig. 3.4) the AE count rate gradually decrease during plastic deformation, there are no sudden drops or distinct peaks like in the case of compression.

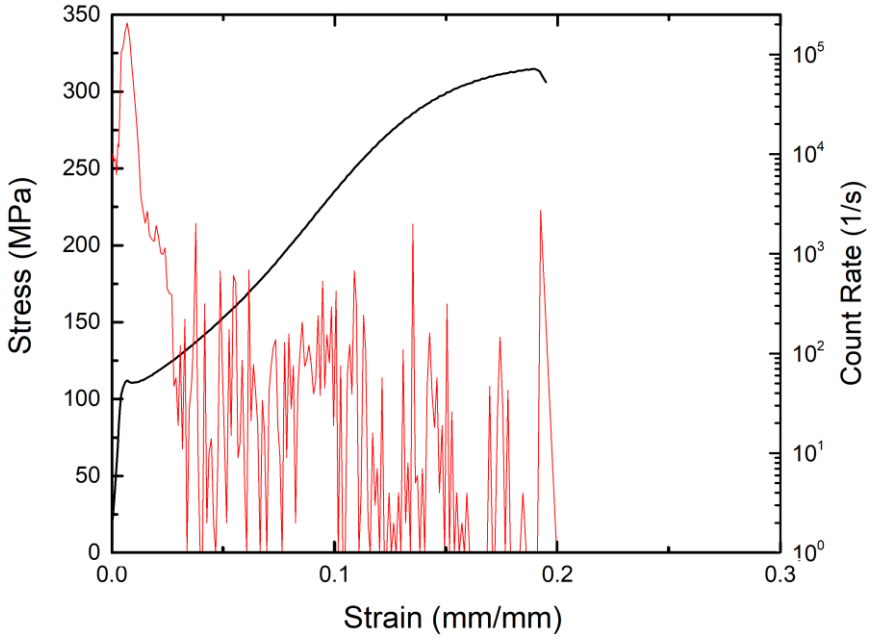

Fig. 3.3: Compressive deformation curve of ZX10 alloy in initial state correlated with the AE count rate

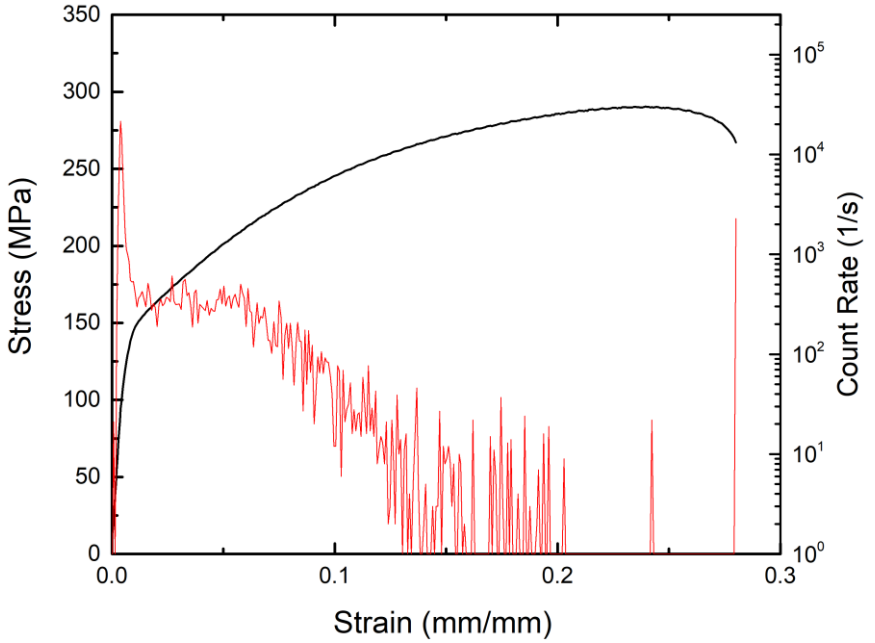

Fig. 3.4: Tensile deformation curve of the ZX10 alloy in initial state correlated with the AE count rate

The microstructure of ZX10 alloy in as extruded state is presented in Fig. 3.5. It can be seen that there are no twins in initial state. Some twinning was also observed in samples subjected to tension up to fracture, as can be seen in Fig. 3.6. However, there is significantly more twinning in samples subjected to pre-compression compared to samples subjected to tension up to fracture.

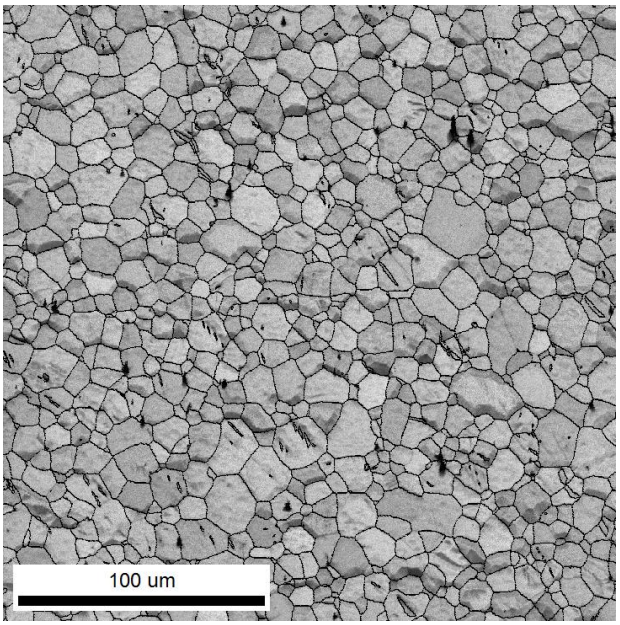

Fig. 3.5: EBSD image quality map with highlighted grain boundaries of as-received ZX10 alloy (× ED).

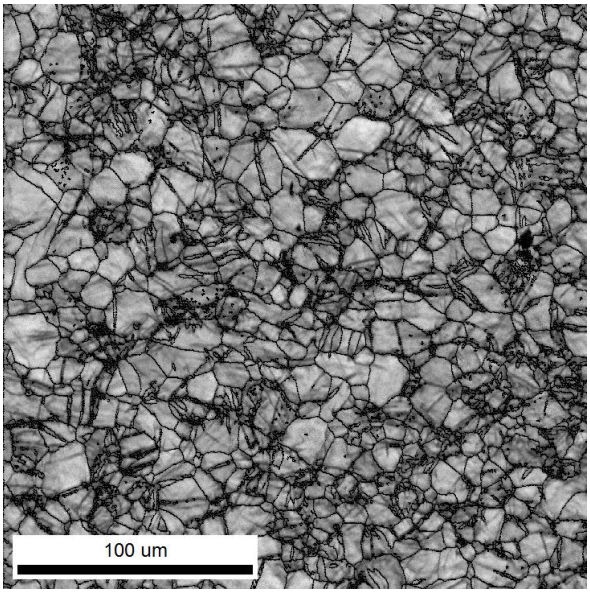

Fig. 3.6: EBSD image quality map with highlighted grain and twin boundaries of as-received ZX10 alloy after tension up to fracture (× ED).

Deformation curves of samples after pre-compression to 140 MPa and subsequent isothermal aging at 150°C for 4, 16, 32 and 64 hours are displayed in Fig. 3.7. Achieved values of compressive yield strength (YS) are presented in Table 3.1. The highest value of YS was achieved by aging time of 16 h and longer aging time led to stress softening. Therefore, in order to investigate the influence of pre-

compression, further experiments were conducted using isothermal aging at 150°C for 16 h (hereafter 16h@150C).

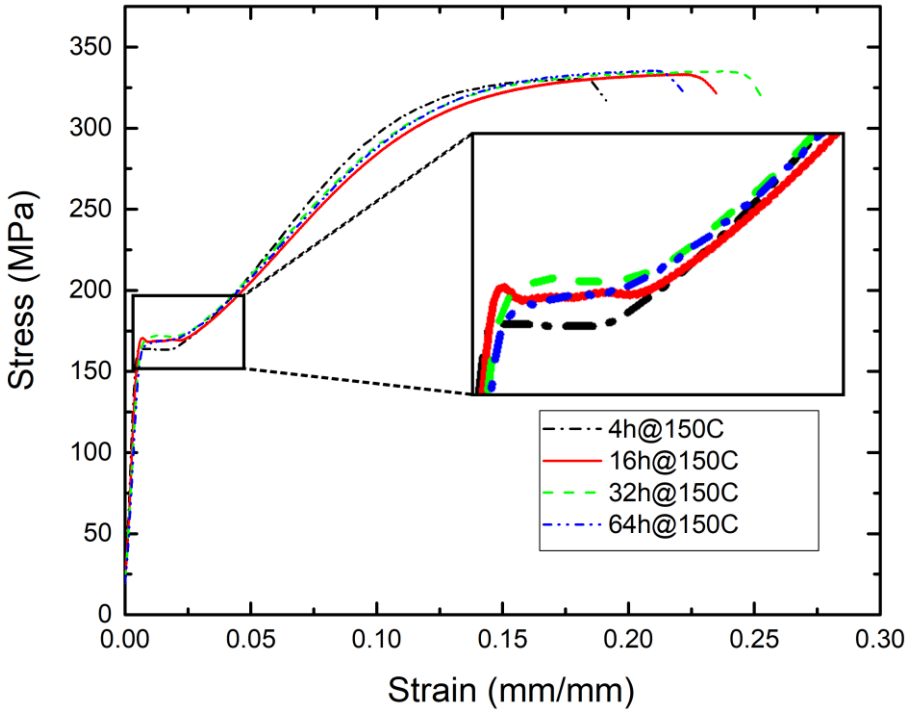

Fig. 3.7: Influence of isothermal aging on deformation behaviour of pre-compressed samples up to 140 MPa

Table 3.1: Compressive YS for the ZX10 alloy after pre-compression of 140 MPa and various aging times

Aging time (h)	4	16	32	64
Compressive YS (MPa)	164 ± 3	**175 ± 4**	168 ± 3	165 ± 3

Deformation curves of samples after isothermal aging for 16 h at 150C (Fig. 3.8 *a)* compression and *b)* tension) are comparable to those for initial samples. An increase in YS after HT in both compression and tension was observed, Table 3.2 and 3.3. However, in tension the increase in YS is significantly higher than in compression. Furthermore, we observe a plateau after yield point (YP) during tensile deformation of sample after HT, Fig. 3.8 b).

The main aim of pre-compression is to introduce the twin boundaries into microstructure. Therefore, in order to achieve partially twinned microstructure, the level of pre-compression should be slightly above compression YS of samples in initial state. Compression curves of samples subjected to pre-deformation without HT (Fig. 3.9 a) show that values of YS are slightly lower than the level of pre-compression (Table 3.2). Compressive deformation curves after pre-compression (Fig. 3.9 a) do not show plateau after yielding. Fig. 3.9 b) displays tensile deformation curves of ZX10 alloy after only pre-compression. The "S" shape of tensile deformation curves of samples subjected to only pre-compression is more pronounced with increasing level of pre-compression (Fig. 3.9 b).

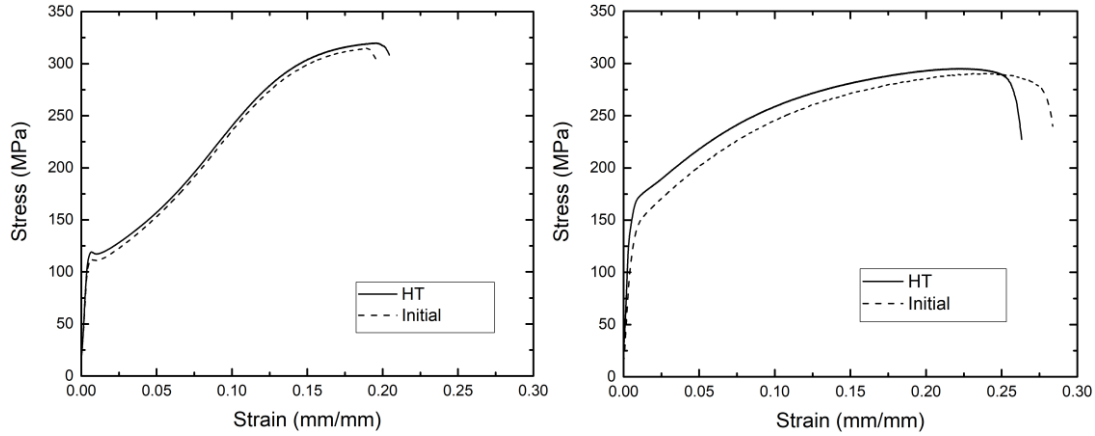

a) b)

Fig. 3.8: Influence of HT (16h@150C) on deformation behaviour in (a) compression and (b) tension

Table 3.2: Compressive YS for the ZX10 alloy in initial state, after HT, after solely pre-compression, and after pre-compression with subsequent HT

	Initial	**After HT**	**Level of pre-compression**	**After pre-compression**	**After pre-compression & HT**
Compressive YS (MPa)	112±2	118±2	130	127±2	165±3
			140	138±3	175±4
			155	152±3	185±4

Table 3.3: Tensile YS for ZX10 alloy in initial state, after HT, after solely pre-compression and after pre-compression with subsequent HT

	Initial	After HT	Level of pre-compression	After pre-compression	After pre-compression & HT
Tensile YS (MPa)	127±3	152±3	130	93±2	108±2
			140	99±2	117±2
			155	104±2	125±3

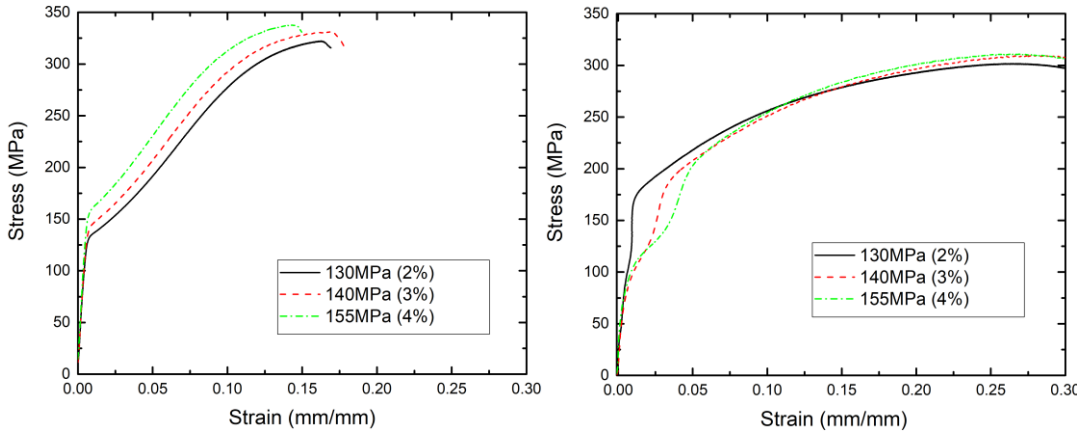

a) b)

Fig. 3.9: Influence of pre-compression on deformation behaviour in (a) compression and (b) tension of as-extruded ZX10 alloy.

Fig. 3.10 displays compressive (a) and tensile (b) deformation curves of samples subjected to pre-compression and subsequent HT (16h@150C). All compression curves exhibit plateau after yielding (Fig. 3.10 a). Furthermore, the “S” shape of samples subjected to pre-compression and HT in tensile deformation (Fig. 3.10 b) is more pronounced compared to those after pre-compression only (Fig. 3.9 b).

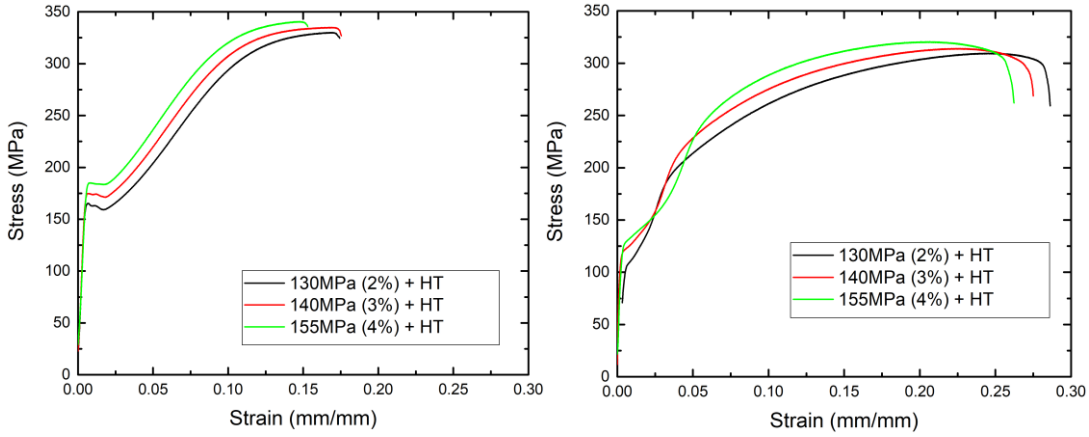

a) b)

Fig. 3.10: Influence of pre-compression and subsequent HT (16h@150C) on deformation behaviour in (a) compression and (b) tension.

Values of compressive YS (red) and tensile YS (green) for samples subjected to HT after pre-strain with respect to level of pre-compression are plotted in Fig. 3.11. Value of YS in tension was significantly lower after pre-compression up to 130MPa and HT comparing to that for sample in initial state. Nevertheless, values of YS for samples in tension increases with increasing level of pre-compression (Table 3.3, Fig. 3.11). For sample after pre-compression up to 155MPa and HT value of tensile YS is comparable to that for sample in initial state.

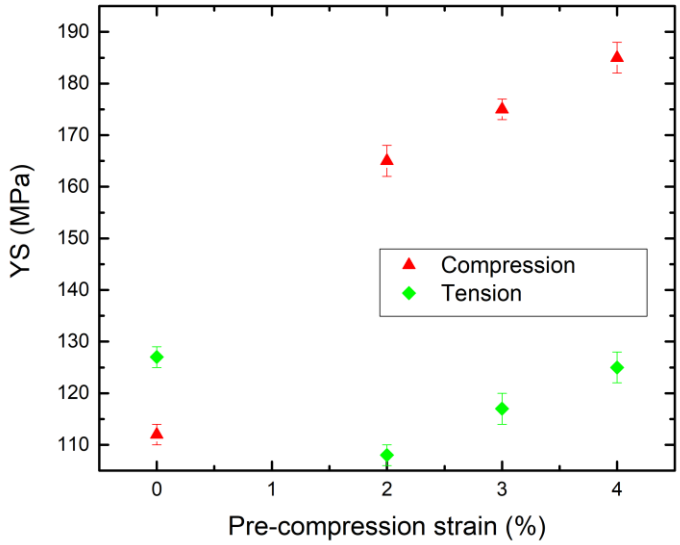

Fig. 3.11: Tensile and Compressive YS after thermomechanical treatment with respect to the level of pre-compression.

To study influence of pre-compression on mechanical properties of investigated material TVF was estimated. The calculated TVF values together with EBSD image quality maps of all investigated samples with highlighted grain (black) and twin (red) boundaries are presented in Fig. 3.12. It can be seen that TVF increases with the increase level of pre-compression. Moreover, values of TVF are slightly lower in samples subjected to HT after pre-compression than those for samples after pre-compression only.

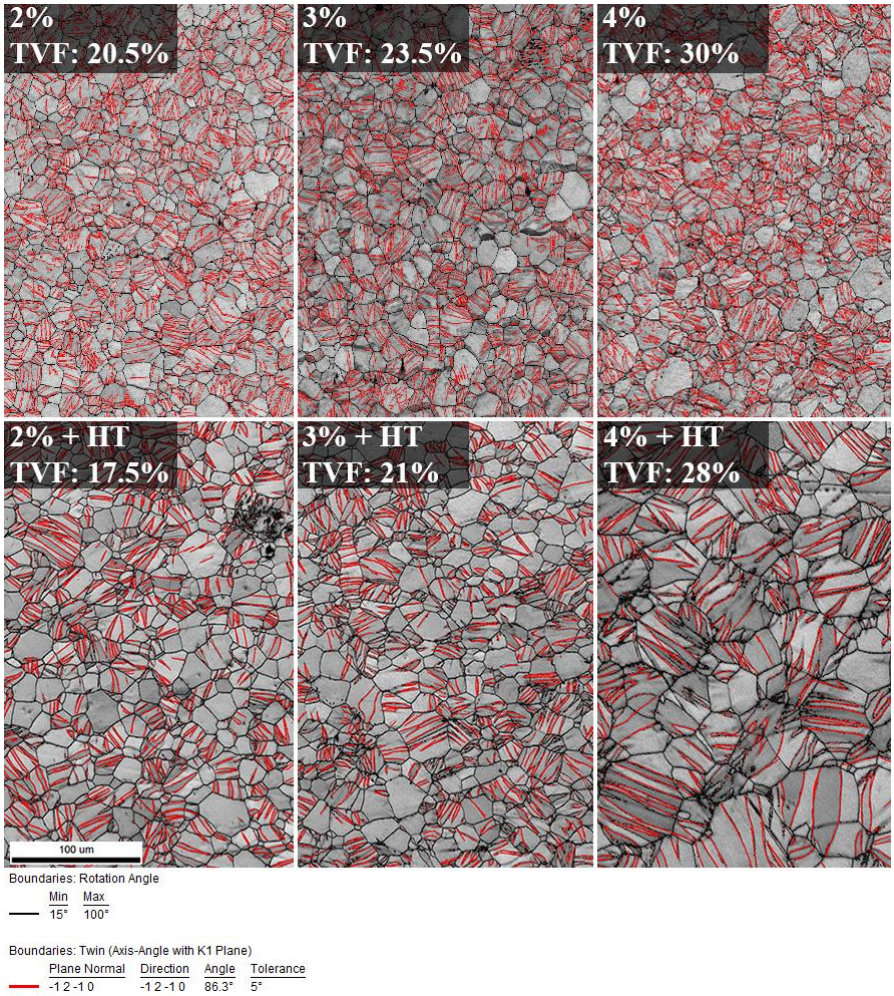

Fig. 3.12: EBSD image quality maps with highlighted grain (black) and tensile twin (red) boundaries together with calculated TVF of samples subjected to thermomechanical treatment (× ED).

KAM analysis of microstructure of all investigated samples is displayed in Fig. 3.13. The KAM is higher in samples subjected to higher levels of pre-compression both before and after HT. We can also see higher overall KAM in samples subjected

to pre-compression only. Furthermore, we observed the clusters with elevated levels of KAM focused around the twin (highlighted red) and grain (highlighted black) boundaries in samples subjected to pre-compression only. In samples after HT, there is no apparent clustering of high KAM near twin and grain boundaries and the KAM seems to be distributed more equally throughout the grain.

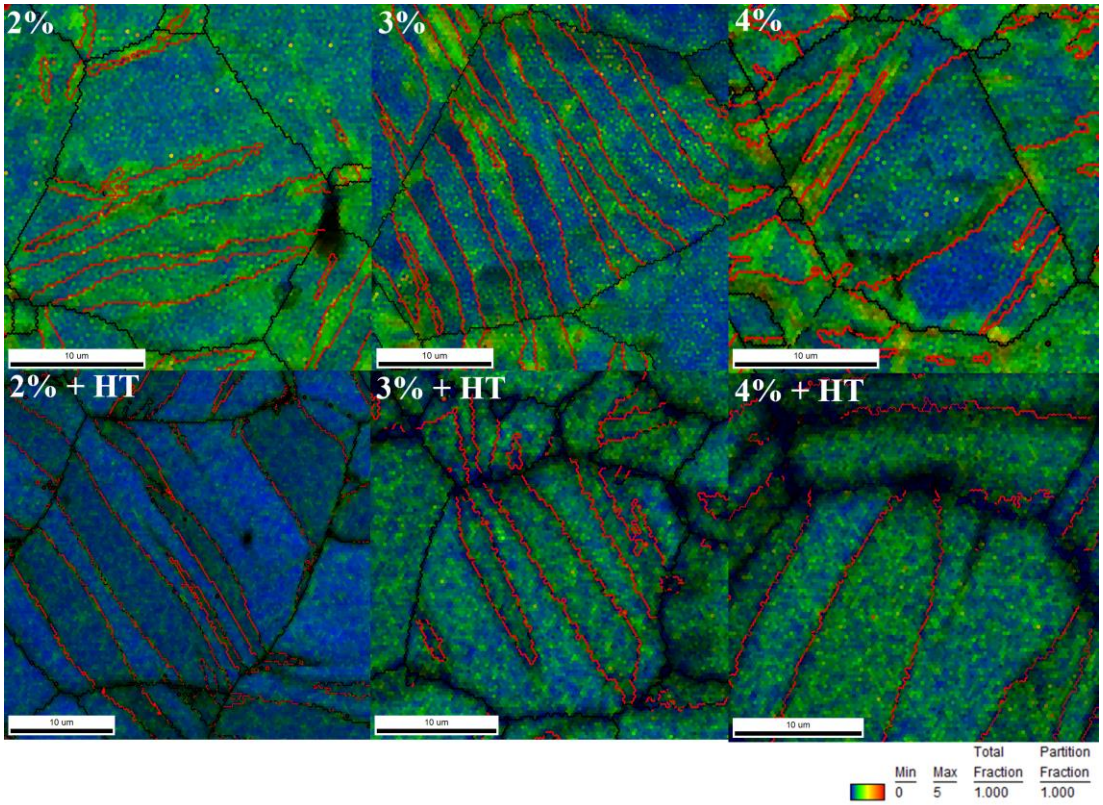

Fig. 3.13: KAM analysis of microstructure of samples subjected to thermomechanical treatment (× ED).

5. Discussion

The tension-compression yield strength asymmetry during loading along ED of sample in initial condition (Fig. 3.2) can be explained by a twin nucleation and strong basal texture of investigated alloy (Fig. 2.1). It is known that extension twinning is orientation dependent process and twins preferentially occurs when loading axis is parallel to ED [13, 18]. Our EBSD measurements confirm significant occurrence of twinning after pre-compression (Fig. 3.12). On the contrary, (Fig. 1.6), plastic deformation during tension proceeds mainly by dislocations in basal <a> and pyramidal <c+a> slip systems [23]. This fact is in a good agreement with our AE measurements. In case of compression (Fig. 3.3), we observed a peak in the AE count rate, which can be related to massive twin nucleation, as an excellent source of AE [24]. Growing of existing twins does not produce detectable AE [20] and further occasional peaks in the AE count rate can be associated with further nucleation of twins in favourable oriented grains for twinning. In tension (Fig. 3.4), we observed a significantly lower peak in the AE count rate than that in compression, which can be explained mainly by a massive multiplication of dislocation. Further decrease of the AE count rate is associated with a decrease in the free path of the moving dislocations. However, in case of polycrystalline material, orientations of some grains and influence of neighbouring grains can led to nucleation of extension twins even during tensile loading along ED [25]. EBSD measurements of sample after tension up to fracture (Fig. 3.6) show significantly less twinning than that after pre-compression (Fig. 3.12). It is important to note that beside extension twins other twin systems can be activated in Mg alloys at higher stress. However, analysis of twin variant is beyond of present work. Therefore, it can be concluded that twining is not dominant deformation mechanism in tension and for introducing twins into microstructure compression as a pre-strain mode is applied. For further development of thermo-mechanical treatment, it is necessary to set the proper conditions of isothermal aging, which will be applied after pre-strain part.

The temperature of heat treatment (150°C) was chosen based on our previous research concerning the same ZX10 alloy [26], where it was shown that higher aging temperature of 200°C after pre-compression lead to softening of the material. Investigation results of influence of isothermal aging on deformation behaviour (Fig. 3.7) provided us information about optimal aging time of 16h, as such HT resulted in

highest value of YS. Samples subjected to HT only before deformation tests, exhibit improvement in both compressive and tensile YS (Table 3.2 and Table 3.3). This can be explained by Mg_2Ca precipitation that is commonly observed in Mg-Zn-Ca alloys, for example in [27, 28]. This studies show that these precipitates are formed on basal planes and have shape of short uniformly dispersed rods. Moreover, in [29] it was shown that HT at 150°C for 10 h resulted in increased Vickers hardness of the ZX10 alloy, what is in good agreement with our results.

Samples subjected to pre-compression only (Table 3.2) exhibit significant increase of compressive YS values. This is characteristic for Mg alloys and for example similar increase of compressive YS after pre-compression in ED was observed in AZ31 alloy in [29]. Slight decrease of YS values from the level of pre-compression is caused by stress relaxation effect. Absence of plateau after yielding (Fig. 3.9a) in those samples can be explained by the growth of existing twins rather than nucleation of new twins.

Pre-compression of samples subjected for tensile tests lead to significant drop in YS (Table 3.3). Similar drop in tensile YS values was observed in pre-compressed AZ31 alloy [30]. This decrease in YS can be explained by detwinning, which takes place at early stages of deformation. Stress requested for propagation of twin boundaries is lower than that for nucleation of new twins [31]. Therefore, reverse tensile loading of extruded Mg alloys previously deformed in compression along ED leads to detwinning process. Twinning- detwinning process during cyclic loading has been recently reported in [18, 32]. The increasing significance of the “S” shape with level of pre-compression in samples subjected to tensile loading (Fig. 3.9 b) can be explained by difference in detwinning process. It is clear from Fig. 3.12 that higher level of pre-compression lead to higher TVF. Subsequently for complete detwinning process higher level of reverse load is necessary to apply. Similar results were presented in [33].

Heat treatment after pre-compression is aimed at precipitation segregation at twin boundaries and a reduction of a number of dislocations in the alloy. As we can see from KAM analysis (Fig. 3.13), clusters of increased KAM are focused around twin and grain boundaries in pre-compressed samples. Those clusters tend to be more intense with increasing level of pre-compression. KAM values are significantly lower in samples subjected to HT after pre-compression and it is no longer localized at twin

and grain boundaries. Thus, isothermal aging leads to redistribution of internal stress in the grains. This effect is most significant in sample with pre-compression level of 2%. As we can see from Table 3.2, the initial compressive YS increased by $\Delta YS = 6$ MPa after HT only, by $\Delta YS = 15$ MPa after only pre-compression of 130 MPa and by $\Delta YS = 53$ MPa after pre-compression of 130 MPa and subsequent HT. Resulting compressive YS after thermomechanical treatment is not a simple superposition of HT and pre-compression contribution but more complex mechanism. This is common for all pre-compression levels. Therefore, more complex process takes place and needs further investigation. Samples subjected to HT after pre-compression also exhibit plateau after yielding (Fig. 3.10 a). This behaviour can be explained by the precipitation segregation at twin boundaries. Precipitation segregation at twin boundaries in magnesium alloys was studied in detail during annealing in recent in-situ TEM study [34]. It was found that this process can affect the mobility of twin boundaries. If the mobility of twin boundaries nucleated during pre-compressions is suppressed, further nucleation of new twins is needed for proceeding of plastic deformation resulted in plateau after yielding. Similar increase of compressive YS after pre-compression and subsequent HT was observed in extruded AZ31 alloy [35].

Situation for tension after thermomechanical treatment is significantly different. Value of YS decreases after applying thermomechanical treatment: YS is (127±3) and (108±2) MPa for sample in initial state and after pre-compression up to 130 MPa with subsequent HT, respectively (Fig. 3.11). This decrease might be due to similar reasons, which were already discussed for samples subjected to pre-compression only. Similar to pre-compression only samples, YS values increase with higher level of pre-compression (Fig. 3.11). At pre-compression level of 155 MPa and subsequent HT the tensile YS increases up to (125±3) MPa (Table 2.3). Increasing of tensile YS with increased pre-compression level is also correlated to increase TVF (Fig. 3.12) and detwinning process as was discussed above. The “S” shape of deformation curves of samples subjected to pre-compression and HT is much more pronounced (Fig. 3.10 b) than those after pre-compression only (Fig. 3.9 b). This might be caused by precipitation segregation at twin boundaries. It is suggested that segregated precipitates at twin boundaries suspend the twin boundary motion until certain level of stress is reached after which the detwinning process begins.

However, it is important to note that applying thermo-mechanical treatment of pre-compression up to 4% of strain with subsequent isothermal aging results in same tensile YS and significantly higher compressive YS comparing to values for sample in as-extruded state.

Conclusions

Investigated ZX10 alloy exhibits tension-compression YS asymmetry in initial condition, what is a common behaviour for extruded Mg alloys. AE measurements helped to determine active deformation mechanisms in compression and tension.

The dependence of aging time on compressive YS of extruded ZX10 alloy was investigated by series of deformation tests conducted on pre-compressed (up to 140MPa) samples. Value of YS after pre-compression without HT was determined to be (138±3) MPa. The highest value of compressive YS (175±4) MPa was achieved with aging time of 16h at 150°C.

Pre-compression without HT resulted in increase of YS in compression and decrease of YS in tension. With increasing level of pre-compression both compressive and tensile YS improve. The "S" shape of tensile deformation curves become more significant with increasing level of pre-compression. This is caused by detwinning process and higher TVF in samples with higher levels of pre-compression.

Pre-compression with subsequent optimized HT resulted in improvement of YS in both tension and compression, when compared to samples subjected to pre-compression only. Compressive YS improved from initial (112±2) MPa to (165±3) MPa and tensile YS to (108±2) MPa, for samples subjected to pre-compression of 130MPa. The highest values of YS were achieved with pre-compression up to 155MPa and HT: (185±4) MPa for compression and YS (125±3) MPa for tension. Therefore, we effectively improved compressive YS without significant negative impact on tensile YS.

Achieved results showed that thermomechanical treatment has a big potential for developing of Mg alloys.

Bibliography

[1] **C. E. Housecroft, A. G. Sharpe.** *Inorganic Chemistry (3rd ed.).* s.l. : TSB, 2008.

[2] **P. Dobroň.** *Štúdium mechanických a fyzikálnych vlastností nových konštrukčných materiálov na báze horčíka metódou akustickej emisie. PhD thesis.* s.l. : MFF UK, 2007.

[3] **J. Brož, V. Roskovec, M. Valouch.** *Fyzikální a matematické tabulky.* s.l. : Nakladatelství technické literatury, 1980.

[4] **J. R. Cameron, J. G. Skofronick, R. M. Grant.** *Physics of the Body. 2nd Edition.* s.l. : Medical Physics Publishing, 1999.

[5] **J. Hofstetter, M. Becker, E. Martinelli, A.M. Weinberg, B. Mingler, H. Kilian, S. Pogatscher, P.J. Uggowitzer, J.F. Loffler.** *High-Strength Low-Alloy (HSLA) Mg–Zn–Ca Alloys with Excellent Biodegradation Performance.* s.l. : Springler, 2014.

[6] **J. P. Hirth, J. Lothe.** *Theory of dislocations (2 ed.).* s.l. : Krieger Pub Co., 1992.

[7] **P. Kratochvíl, P. Lukáč, B. Sprášil.** *Úvod do fyziky kovů I.* s.l. : SNTL, 1984.

[8] **P. Minárik.** *Effect of Composition and Microstructure on Mechanical and Corrosion Properties in Magnesium Alloys with a Potential for Medical Applications, PhD thesis.* s.l. : MFF UK, 2014.

[9] **M. M. Avedesian, H. Baker.** *ASM specialty handbook: magnesium and magnesium alloys.* s.l. : ASM international, 1999.

[10] **R. Mises.** *Mechanik der plastischen Formaenderung von Kristallen.* s.l. : Zeitschrift für Angewandte Mathematik und Mechanik 8, 1928.

[11] **W. D. Callister.** *Materials Science and Engineering, An Introduction.* s.l. : John Wiley & Sons, Inc., 2006.

[12] **D. Drozdenko.** *Study of novel magnesium alloys with controlled microstructure and texture, PhD. Thesis.* s.l. : MFF UK, 2016.

[13] **W. Wu, H. Qiao, K. An, X. Guo, P. Wu, P. K. Liaw.** *Investigation of deformation dynamics in a wrought magnesium alloy.* s.l. : International Journal of Plasticity, 2014.

[14] **L. Wu, A. Jain, D.W. Brown, G.M. Stoica, S.R. Agnew, B. Clausen, D.E. Fielden, P.K. Liaw.** *Twinning–detwinning behavior during the strain-controlled low-cycle fatigue testing of a wrought magnesium alloy, ZK60A.* s.l. : Acta Materialia 56, 2007.

[15] **V. Vlack.** *A Textbook of Materials Technology, 1st edittion.* s.l. : Pearson Education Inc., 1973.

[16] **S. R. Kalidinidi, A. A. Salem, R. D. Doherty.** *Role of Deformation Twinning on Strain Hardening in Cubic and Hexagonal Polycrystalline Metals.* s.l. : Advanced Engeneering Materials, 2003.

[17] **A. Keyhani, R. Roumina.** *Quantification of Dislocation-Precipitate Interactions.* 2017.

[18] **D. Drozdenko, J. Bohlen, S Yi, P. Minárik, F. Chmelík, P. Dobroň.** *Investigating a twinning-detwinning process in wrought Mg alloys by the acoustic emission technique.* s.l. : Acta Materialia, 2016.

[19] **C. R. Heiple, S. H. Carpenter.** *Acoustic Emission Produced by Deformation of Metals and Alloys – A Review: Part I.* s.l. : Journal of Acoustic Emission 6, 1987.

[20] **J. P. Toronchuk.** *Acoustic emission during twinning of zn single crystals.* s.l. : Materials Evaluation, 1977.

[21] **ASTM.** *Standard Practice for Acoustic Emission Examination of Fiberglass Reinforced Plastic Resin (FRP) Tanks/Vessels.* 2011. E1067/E1067-M-11.

[22] **S. Lax.** *Kernel Average Misorientation Confidence Index Correlation from FIB Sliced NiFe-Cr.* s.l. : Microscopy Society of America, 2011.

[23] **J.B. Lin, W.J. Ren, X.Y. Wang, L.F. Ma.** *Tension–compression asymmetry in yield strength and hardening behaviour of as-extruded AZ31 alloy.* s.l. : Materials Science and Technology, 2016.

[24] **C. R. Heiple, S. H. Carpenter.** *Acoustic Emission Produced by Deformation of Metals and Alloys – A Review: Part II.* s.l. : Journal of Acoustic Emission 6, 1987.

[25] **I.J. Beyerlein, C.N. Tomé.** *A dislocation-based constitutive law for pure Zr including temperature effects.* s.l. : International Journal of Plasticity, 2008.

[26] **D. Drozdenko, P. Dobroň, J. Olejňák, M. Hegedüs, K. Horváth, J. Bohlen.** *Mechanical properties of thermo-mechanically treated extruded Mg-Zn-based alloys.* s.l. : Magnesium Technology , 2018.

[27] **K. Oh-ishi, R. Watanabe, C.L. Mendis, K. Hono.** *Age-hardening response of Mg–0.3 at.%Ca alloys with different Zn contents.* s.l. : Materials Science and Engineering A, 2009.

[28] **J. Nie.** *Precipitation and Hardening in Magnesium Alloys.* s.l. : The Minerals, Metals & Materials Society and ASM International, 2012.

[29] **J. J. He, T. M. Liu, H. B. Chen, L. W. Lu, F. S. Pan.** *Effects of prior compression on ductility and yielding behaviour in extruded magnesium alloy AZ31.* s.l. : Materials Science and Technology, 2013.

[30] **L. Wang, G. Huang, Q. Quan, P. Bassani, E. Mostaed, M. Vedani, F. Pan.** *The effect of twinning and detwinning on the mechanical property of AZ31 extruded magnesium alloy during strain-path changes.* s.l. : Materials and Design, 2014.

[31] **J.W.Christian, S.Mahajan.** *Deformation twinning.* s.l. : Progress in Materials Science, 1995.

[32] **Y.N.Wang, J.C.Huang.** *The role of twinning and untwinning in yielding behavior in hot-extruded Mg–Al–Zn alloy.* s.l. : Acta Materialia, 2007.

[33] **J. Bohlen, P. Dobron, L. Nascimentoa, K. Parfenenko, F. Chmelik.** s.l. : Acta Physica Polonica A, 2012.

[34] **D. Guan, J. Nutter, J. Sharp, J. Gao, W. M. Rainforth.** *Direct observation of precipitation along twin boundaries and dissolution in a magnesium alloy annealing at high temperature.* s.l. : Scripta Materialia, 2017.

[35] **Y. Xin, Y. Zhang, H. Yu, H. Chen, Q. Liu.** *The different effects of solute segregation at twin boundaries on mechanical behaviors of twinning and detwinning.* s.l. : Materials Science & Engineering A, 2015.

List of Tables

Table 3.1: Compressive YS for the ZX10 alloy after pre-compression of 140MPa and various aging times

Table 3.2: Compressive YS for the ZX10 alloy in initial state, after HT, after solely pre-compression, and after pre-compression with subsequent HT

Table 3.3: Tensile YS for ZX10 alloy in initial state, after HT, after solely pre-compression and after pre-compression with subsequent HT

List of Abbreviations

AE – acoustic emission

BSE - Backscattered electron

c, a – lattice constants of HCP lattice

CRSS - critical resolved shear stress

d - average grain size

EBSD – electron backscatter diffraction

ED - extrusion direction

ER - extrusion ratio

HCP - hexagonal close packed

KAM – kernel average misorientation

RT – room temperature

SEM – scanning electron microscopy

TEM – transmission electron microscopy

TVF – twin volume fraction

YP – yield point

YS – yield strength

τ - shear stress